ISSN 1674-1056
http://cpb.iphy.ac.cn
http://iopscience.iop.org/cpb
中国物理 B
Chinese Physics
中国物理
Chinese Physics B

Structure, conductivity, and ion emission properties of $RbAg_4I_5$ solid electrolyte film prepared by pulsed laser deposition

Jun-Lian Chen(陈军联), Wen-Bin Zuo(左文彬), Xian-Wen Ke(柯贤文), Alexander B Tolstoguzov, Can-Xin Tian(田灿鑫), Neena Devi, Ranjana Jha, Gennady N Panin, De-Jun Fu(付德君)

Citation: Chin. Phys. B . 2019, 28(6): 060705. **doi:** 10.1088/1674-1056/28/6/060705
Journal homepage: http://cpb.iphy.ac.cn; http://iopscience.iop.org/cpb

What follows is a list of articles you may be interested in

High temperature thermoelectric properties of highly c-axis oriented $Bi_2Sr_2Co_2O_y$ thin films fabricated by pulsed laser deposition

Chen Shan-Shan, Wang Shu-Fang, Liu Fu-Qiang, Yan Guo-Ying, Chen Jing-Chun, Wang Jiang-Long, Yu Wei, Fu Guang-Sheng

Chin. Phys. B . 2012, 21(8): 087306. **doi:** 10.1088/1674-1056/21/8/087306

Structure, conductivity, and ion emission properties of $RbAg_4I_5$ solid electrolyte film prepared by pulsed laser deposition*

Jun-Lian Chen(陈军联)[1,2], Wen-Bin Zuo(左文彬)[2], Xian-Wen Ke(柯贤文)[1], Alexander B Tolstoguzov[3], Can-Xin Tian(田灿鑫)[4], Neena Devi[1,5], Ranjana Jha[5], Gennady N Panin[6], and De-Jun Fu(付德君)[2,†]

[1] *School of Printing and Packaging, Wuhan University, Wuhan* 430072, *China*
[2] *Shenzhen Institute of Wuhan University, A302 Research Bldg., No. 6 Aoxin 2nd Rd., Nanshan Hitech Zone, Shenzhen* 518057, *China*
[3] *Ryazan State Radio Engineering University, Gagarin Str.* 59/1, 390005 *Ryazan, Russia*
[4] *School of Physics and Technology, Lingnan Normal University, Zhanjiang* 524048, *China*
[5] *Department of Physics, Netaji Subhas Institute of Technology, University of Delhi, Dwarka Sector-3, New Delhi* 110078, *India*
[6] *Institute of Microelectronics Technology, Russian Academy of Sciences, Chernogolovka, Moscow* 142432, *Russia*

(Received 14 February 2019; revised manuscript received 18 March 2019; published online 8 May 2019)

We fabricated a silver ion emitter based on the solid state electrolyte film of $RbAg_4I_5$ prepared by pulsed laser deposition. The $RbAg_4I_5$ target for PLD process was mechano-chemically synthesized by high-energy ball milling in Ar atmosphere using β-AgI and RbI as raw materials. The ion-conducting properties of $RbAg_4I_5$ were studied by alternating current (AC) impedance spectroscopy and the ionic conductivity at room temperature was estimated 0.21 S/m. The structure, morphology, and elemental composition of the $RbAg_4I_5$ film were investigated. The Ag^+ ion-conducting property of the prepared superioni-conductor film was exploited for ion–beam generation. The temperature and accelerating voltage dependences of the ion current were studied. Few nA current was obtained at the temperature of 196 °C and the accelerating voltage of 10 kV.

Keywords: $RbAg_4I_5$, ball milling, solid state electrolyte film, ion–beam source, ionic conductivity

PACS: 07.77.Ka **DOI:** 10.1088/1674-1056/28/6/060705

1. Introduction

Solid state electrolytes (SSEs) represent a class of materials with ionic conductivity owing to the fast transport paths for the mobile ions inside them. In 1961, Reuter *et al.* reported SSEs of Ag_3SI and Ag_3SBr with the ionic conductivity of 10^{-2} S/cm at 25 °C, which breaks the restrictions on the application of SSEs because of their high ionic conductivity ($\gg 10^{-6}$ S/cm at 25 °C).[1] Since then, dozens of different solid state electrolyte materials have been reported, such as Ag^+-conducting halide ($RbAg_4I_5$[2] and α-AgI[3]), oxygen ion-conducting $CaO:ZrO_2$,[4] and $ThO_2:Y_2O_3$,[5] and sodium-conducting β-Al_2O_3.[6] There are many advantages of SEs, including high ionic conductivity, wider temperature range for conduction than liquid electrolyte and easy miniaturization owing to the solid form, and the dominating charge carriers in SSEs being ions with the insignificant electronic conductivity.[7] Hence, solid electrolytes have been widely used in new-type solid state battery,[8–10] high-temperature solid-oxide fuel cell,[11] electrochromic devices,[12] memory devices,[13] display devices,[14] and ionic conductivity sensors.[15]

In addition, SSEs are promising candidates in field emission electric propulsion (FEEP) systems, due to their superior features of compactness, long working life, and low power consumption.[16,17] FEEP systems with SSEs can be used on space-constrained micro-spacecraft to enable on-orbit controls such as raising, lowering of its altitude and repositioning of the spacecraft owing to the ability of the source to produce controllable thrust within μN range.[18] For example, emission of oxygen ions from an oxygen ion–beam source with solid-state ion conductor was reported by Wilbur *et al.*[19] in 2005. In addition, continuous silver ions emissions from an Ag^+ ion source based on $(AgI)_{0.5}$–$(AgPO_3)_{0.5}$ SSE was reported by Escher *et al.* in 2006.[20]

$RbAg_4I_5$ was prepared and investigated in the mid-1960s.[18] In 1967, Owens *et al.* revealed that crystalline compound $RbAg_4I_5$ exhibited superior ion conductivity of more than 10^1 S/m at 25 °C with negligible electronic contribution of $< 10^{-9}$ S/cm.[21] Since then, $RbAg_4I_5$ SSEs have been extensively studied. In 2016, Tolstogouzov *et al.*[18] reported an Ag^+ ion–beam source based on $RbAg_4I_5$ solid state electrolyte films, generating stable silver ion currents.

In the present work, the $RbAg_4I_5$ solid state electrolyte film was deposited at the apex of a silver needle by pulsed laser deposition (PLD), constituting an Ag^+ ion emitter. The ion-conducting properties of $RbAg_4I_5$ solid electrolyte were

*Project supported by the National Natural Science Foundation of China (Grant No. 11875210), China Postdoctoral Science Foundation (Grant No. 2018M640724), the International Cooperation Program of Guangdong Provincial Science and Technology Plan Project (Grant No. 2018A050506082), and the Talent Project of Lingnan Normal University, China (Grant No. ZL1931).

†Corresponding author. E-mail: djfu@whu.edu.cn

© 2019 Chinese Physical Society and IOP Publishing Ltd

studied. The characteristics of the point-like ion source were tested and analyzed. As an advanced type of ion emissive device, solid electrolyte ion sources are promising candidates for use in the ion propulsion system of miniature spacecraft with limited on-board payloads.

2. Experimental section

2.1. Preparation of solid electrolyte $RbAg_4I_5$

$RbAg_4I_5$ was synthesized by high-energy ball milling process in Ar atmosphere. Pure powders of β-AgI and RbI were used as raw materials. Desired amounts of β-AgI and RbI (molecular ratio was 4:1) were weighed and mixed in an agate mortar. First, the mixture was ground by an agate pestle for 5 min beforehand to obtain the homogeneous reactants. Then, the mixture powder with numerous 6-mm diameter agate balls was placed in an agate container of 100 ml in volume for milling. Next, the agate container was placed in a stainless steel vacuum sleeve with a hole for pumping and feeding argon. The mechanical milling process was performed in a planetary ball mill (DY-30, Nanjing NANDA), which was rotated at a speed of 380 rpm for 2.5 h. Finally, the ball-milled powders were annealed in argon at 150 °C for 5 h.

The $RbAg_4I_5$ thin film was deposited on the apex of a Ag tip and simultaneously on the Ag substrate by a pulsed laser deposition (PLD) system (PLD-450b, Germany COHERENT). The synthesized $RbAg_4I_5$ powders were pressed into a pellet (target) with a diameter of 30 mm and thickness of 1 mm–2 mm. A KrF laser (GCR-170, Spectra Physics) operated at the wavelength of 248 nm with the maximum energy-per-pulse of 200 mJ was used for irradiation in the pulsed laser system. The laser pulse width and pulse frequency are 30 ns and 5 Hz, respectively, and the laser average power is 0.7 W. The laser beam reflected from a reflective mirror was align to focus on a small zone of the target surface (a circular light spot with diameter of 1 mm–2 mm). The target-substrate distance was 55 mm. The pressure within the vacuum chamber was kept to be 4×10^{-3} Pa. The target was rotated at a speed of 10 rpm driven by a motor. The deposition was carried out for 50 min at the substrate temperature of 80 °C.

2.2. Characterizations

The $RbAg_4I_5$ powder was pressed into a pellet with diameter of 6 mm and thickness of 1 mm–2 mm by an electric press machine (DY-30, Tianjin KEQIGAOXIN), which supplied a molding pressure of 6 MPa for 1 min, then silver electrodes were deposited on both sides of the pellet. The pellet was used for AC impedance measurements, which was conducted from 20 Hz to 1 MHz at various temperatures using an impedance meter (6500B, Wayne Kerr).

The $RbAg_4I_5$ powder and thin film were characterized by x-ray diffraction (XRD) (D8 Advance, BRUKER) using Cu-Kα radiation ($\lambda = 0.1542$ nm) within the 2θ range of 20°–60°. The morphology of the $RbAg_4I_5$ thin film was observed by SEM (SIRION, FEI) equipped with EDS. The elemental composition of the $RbAg_4I_5$ solid electrolyte film was investigated by XPS (ESCALAB 250 Xi, Thermo Fisher) and all the spectra were calibrated with the C 1 s core level spectrum collected at the binding energy of 284.6 eV.

2.3. Construction of the ion source

To test the ion–beam current generated by the silver ion source based on the $RbAg_4I_5$ superionic conductor, an experimental system consisting of an emitter assembly 1, heating device 2, and ion–beam collector 3 was established, as presented in Fig. 1.

The emitter assembly 1 is composed of a silver tip coated with an $RbAg_4I_5$ film by PLD method (ion emitter) and a cylindrical copper (tip holder) in a stainless steel tube. The sliver tip has an apex radius less than 10 μm, machined from a silver rod with a diameter of 6 mm and length of 25 mm. It is screwed together with the cylindrical copper, which is in the stainless steel tube. The non-contact heating device 2 made of nichrome wires is used to heat the stainless steel tube. The steel tube is wrapped around by a layer of mica insulator. The ion–beam collector 3 includes a grounded diaphragm, which is 7.5-mm distant from the tip apex and a Faraday cup, which is connected with a picoammeter. A DC high-voltage power supply provides the positive voltage ranging from 0.1 kV to 20 kV while another power source is for the heating device. The ion-source device works in vacuum with a residual gas pressure of $\sim 10^{-4}$ Pa.

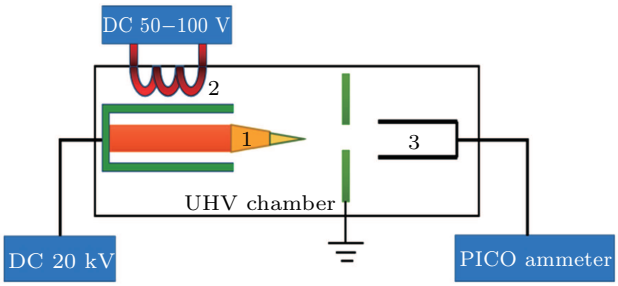


Fig. 1. Schematic diagram of the silver ion–beam source.

3. Results and discussion

3.1. Structure and ionic conductivity of $RbAg_4I_5$

The XRD spectra of the powders obtained by ball-milling of β-AgI and RbI with an agate pestle for 10 min and synthesized after ball milling and subsequent annealing in argon are shown in Fig. 2. It is shown that grinding of the raw materials by an agate pestle for 10 min results in the formation of the $RbAg_4I_5$ phase. In addition, according to JCPDS card No. 83–2045, the AgI phase is still remained. However, there is no other phase but the characteristic peak of pure $RbAg_4I_5$ in the XRD spectrum of synthesized and annealed powders. All

the diffraction peaks can be indexed from JCPDS card No. 74–2390. The sharp and narrow peaks confirm good crystallinity of the obtained β-manganese cubic $RbAg_4I_5$.

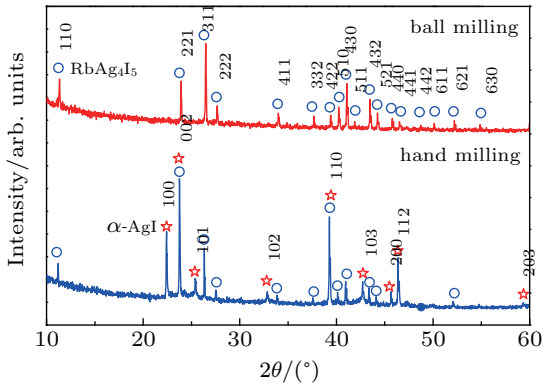


Fig. 2. XRD spectra of the powders obtained by grinding β-AgI and RbI with an agate pestle and synthesized after ball milling and subsequent annealing. Symbols ◯ and ☆ stand for the characteristic peaks of $RbAg_4I_5$ and AgI phases, respectively.

Figure 3(a) shows the AC impedance spectra for $RbAg_4I_5$ at various temperatures of 30 °C–80 °C; the impedance values are determined by the intersecting point of the semicircle with the real axis. It has been calculated that the conductivity of the $RbAg_4I_5$ solid electrolyte at room temperature is 0.21 S/m. Figure 3(b) presents the temperature dependence of the conductivity of $RbAg_4I_5$. The conductivity versus temperature is fitted well by the Arrhenius equation:

$$\sigma = \frac{A}{T}\exp(-E_a/k_BT), \tag{1}$$

where T is the absolute temperature, A the pre-exponential factor, E_a the activation energy for conduction, and k_B the Boltzmann's constant.[22] The fitting gives the activation energy for conduction of $RbAg_4I_5$ as 0.17 eV.

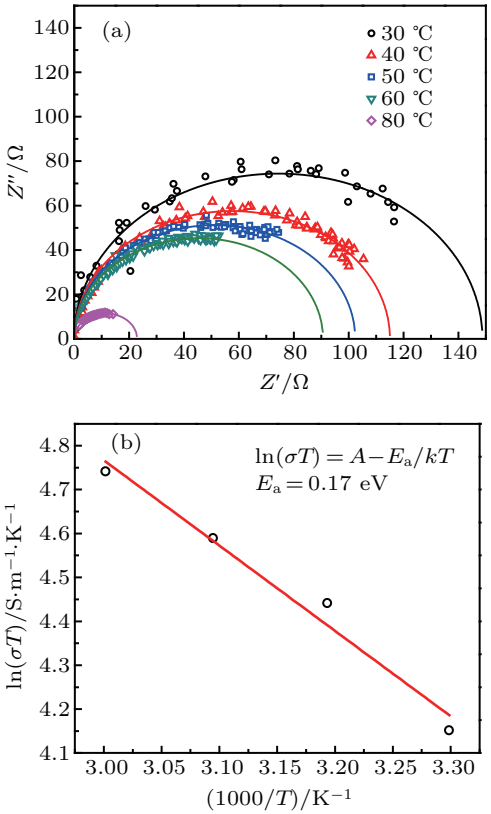


Fig. 3. Temperature dependence of (a) impedance and (b) conductivity of the $RbAg_4I_5$ target.

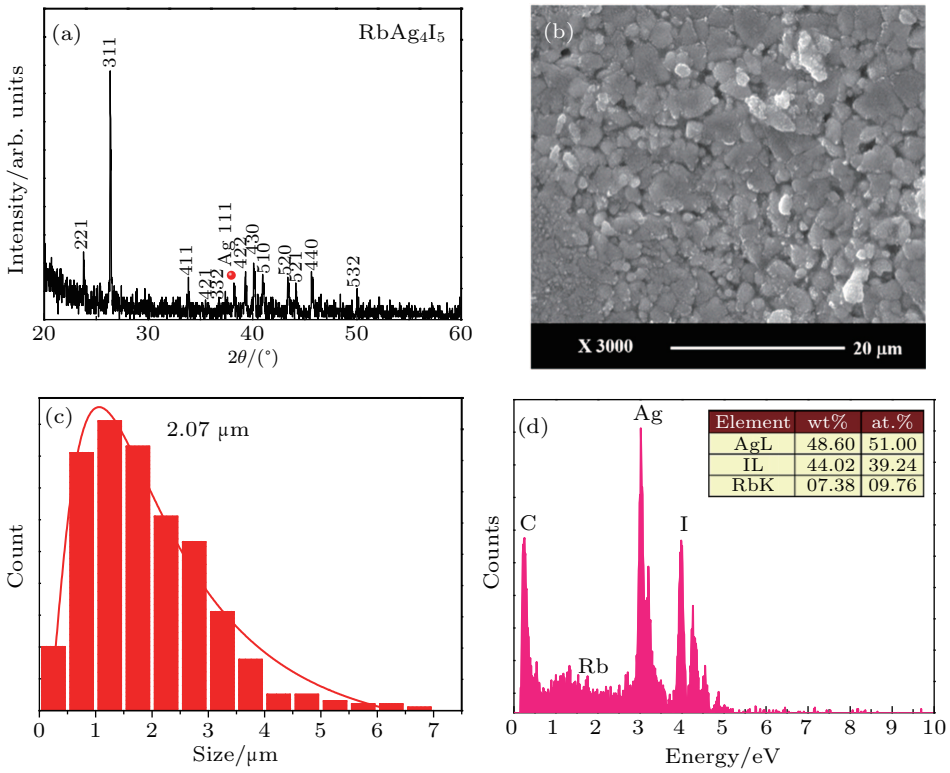


Fig. 4. Characterization of the $RbAg_4I_5$ film: (a) XRD spectrum, (b) SEM image, (c) the particles size distribution, (d) EDS spectrum, the inset shows the elemental composition.

The $RbAg_4I_5$ film was deposited on the Ag substrate at laser energy of 200 mJ and substrate temperature of 80 °C. The XRD pattern is shown in Fig. 4(a). Nearly all the diffraction peaks of $RbAg_4I_5$ can be indexed (JCPDS card No. 74-1416). The diffraction peak at 38.12° indexed to (111) plane of the Ag phase (JCPDS card No. 87-0720) is the strongest diffraction peak of Ag, which is caused by the silver substrate. The XRD result shows that the $RbAg_4I_5$ film is of high purity.

Figure 4(b) shows the SEM morphology of the $RbAg_4I_5$ thin film. The large particles formed from the aggregation of crystalline grains can be observed, indicating a rough surface. It can be seen from Fig. 4(c) that the average particles size of the $RbAg_4I_5$ thin film is 2.07 μm.

Figure 4(d) shows the EDS results of the $RbAg_4I_5$ thin film, revealing the presence of Rb, Ag, and I elements in the sample. The elemental composition is listed in the inset table. It has been calculated that the ratio of Rb:Ag:I in the $RbAg_4I_5$ film is 1:5.23:4.02. The ratio is slightly different from the intended value 1:4:5. The deviation could be attributed to the fact that the element iodine could evaporate easily in the process of pulsed laser deposition leading to a decrease of the portion of iodine.[7]

The elemental composition and chemical bonds in the $RbAg_4I_5$ film were measured by XPS. Figures 5(a)–5(c) show the core level spectra of Rb 3d, Ag 3d, and I 3d, respectively. While Ag and iodine have much separated $3d_{5/2}$ and $3d_{3/2}$ peaks, the two peaks of Rb are overlapped. This happens because the energy levels of Rb $3d_{5/2}$ and $3d_{3/2}$ are very close.

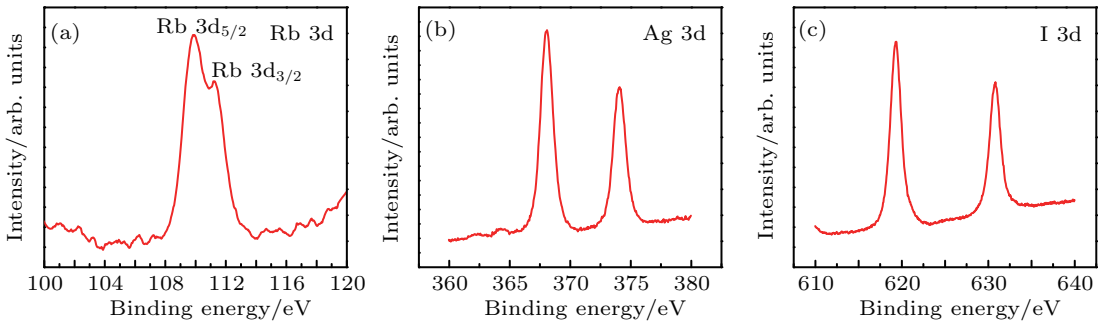


Fig. 5. The core level spectra of (a) Rb 3d, (b) Ag 3d, and (c) I 3d.

3.2. Characteristics of ion emission

Figure 6(a) shows the temperature dependence of ion current emitted by the silver ion–beam source based on the $RbAg_4I_5$ solid state electrolyte film at the accelerating potential of 10 kV. The ion current increases with the increasing of temperature. There is no evident difference between the two current curves measured in the course of heating and cooling the ion source, which shows the good stability and reproducibility of the operation performance of the ion source. Figure 6(b) presents the Arrhenius plot of the ion current versus temperature. Based on the Arrhenius equation mentioned above, the activation energy obtained here is 0.31 eV higher than that obtained from conductivity measurements because it characterizes not only the ionic conductivity (ion-transport process) of solid state electrolyte, but also the ion emission process occurring on its surface.

Figure 7(a) shows the volt–ampere characteristic (I–U_{acc}) of the silver ion source at the working temperature of 196 °C, which shows an increasing tendency in total. When increasing and decreasing the acceleration potential, two I–U_{acc} curves with a hysteresis effect are observed, which results from the inertial character of Ag^+ migration through the $RbAg_4I_5$ solid state electrolyte film.[18]

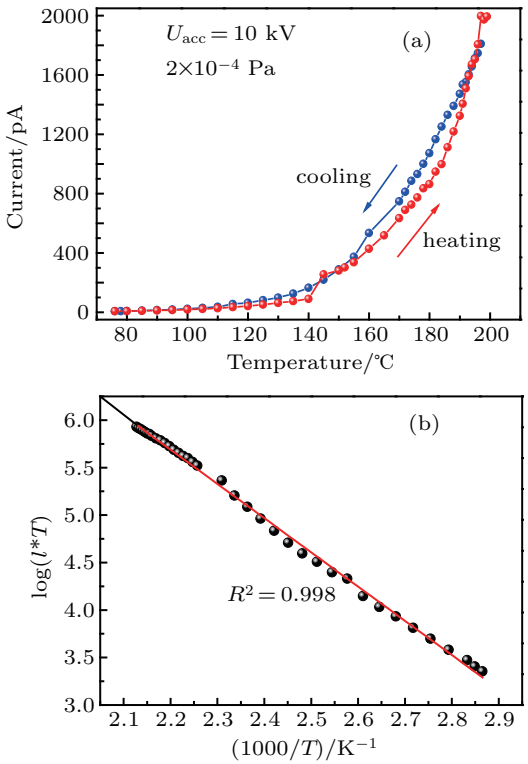


Fig. 6. Temperature dependence of (a) ion current obtained at 10-kV acceleration potential and (b) conductivity of the $RbAg_4I_5$ solid electrolyte film.

A running test of the silver ion source under the heating temperature of 196 °C and 10-kV acceleration potential for

few minutes was conducted, as shown in Fig. 7(b). It can be estimated that the average ion current is about 2 nA.

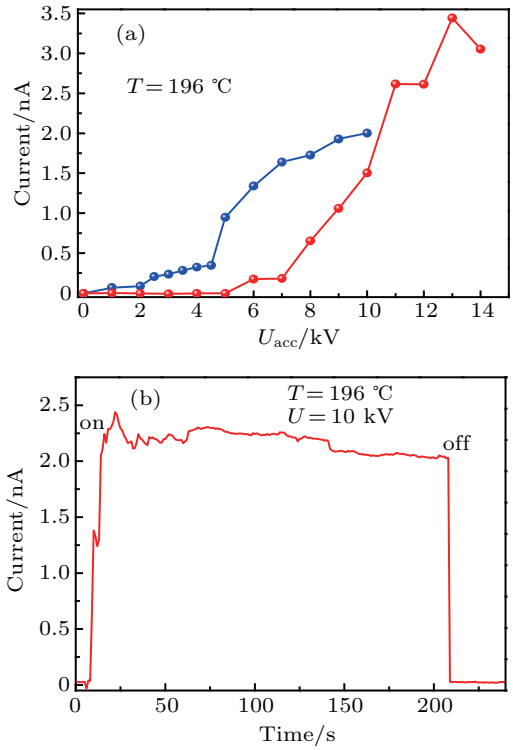


Fig. 7. (a) Volt–ampere characteristic (I–U_{acc}) of the silver ion source under the heating temperature of 196 °C and (b) running test of the silver ion source under the heating temperature of 196 °C and 10-kV acceleration potential for few minutes.

4. Conclusion

Mechano-chemical synthesis of the $RbAg_4I_5$ powder was performed for the PLD process. The pulsed laser deposited film on Ag substrate at temperature of 80 °C exhibited pure $RbAg_4I_5$ phase. The grain structure with the size of 2.07 μm was observed. The AC impedance spectra revealed that the ionic conductivity of the $RbAg_4I_5$ solid state electrolyte was 0.21 S/m at room temperature. The atomic ratio of $RbAg_4I_5$ slightly deviated from the intended value of 1:4:5 because of the evaporation of the element iodine. The ion-conducting property of $RbAg_4I_5$ was exploited for the generation of Ag^+ ion beams. The dependences of ion current on temperature and accelerating potential were established, and an ion current of several nA was obtained at 196 °C and 10-kV potential.

References

[1] Reuter B and Hardell K 1961 *Naturwiss.* **48** 161
[2] Wang P F, Liu Y, Yin J, Ma W Y, Zhu J L, Dong Z M and Sun J L 2019 *Nanotechnol.* **30** 25602
[3] Yoshiasa A, Kanamaru F and Koto K 1988 *Solid State Ionics* **27** 275
[4] Lee D Y and Tseng T Y 2012 *IEEE Electron Dev. Lett.* **33** 803
[5] Cosentino I C and Muccillo R 1997 *Mater. Lett.* **32** 295
[6] Yi E, Temeche E and Laine R M 2018 *J. Mater. Chem. A* **6** 12411
[7] Yang B, Liang X F, Guo H X, Yin K B, Yin J and Liu Z G 2008 *J. Phys. D: Appl. Phys.* **41** 115304
[8] Kim D H, Oh D Y, Park K H, Choi Y E, Nam Y J, Lee H A, Lee S M and Jung Y S 2017 *Nano Lett.* **17** 3013
[9] Gao J, Zhao Y S, Shi S Q and Li H 2016 *Chin. Phys. B* **25** 018211
[10] Wang S F and Chen L Q 2016 *Chin. Phys. B* **25** 018202
[11] Moria M, Tompsettb G M, Sammesc N M, Suda E and Takeda Y 2003 *Solid State Ionics* **158** 79
[12] Yoo S J, Lim J W and Sung Y 2006 *Sol. Energy Mater. Sol. Cells* **90** 477
[13] Huang J Q, Shi L P, Yeo E G, Yi K J and Zhao R 2012 *IEEE Electron Dev. Lett.* **33** 98
[14] Shizukuishi M, Kaga E, Shimizu I, Kokado H and Inoue E 1981 *Jpn. J. Appl. Phys.* **20** 581
[15] Miura N, Nakatou M and Zhuiykov S 2003 *Sens. Actuators B: Chem.* **93** 221
[16] Zuo W B, Pelenovich V, Tolstogouzov A, Zeng X M, Wang Z G, Song X Q, Gusev S I, Tian C X and Fu D J 2019 *J. Alloys Compd.* **790** 109
[17] Tolstoguzov A B, Belykh S F, Gololobov G P, Gurov V S, Gusev S I, Suvorov D V, Taganov A I, Fu D J, Ai Z and Liu C S 2018 *Instrum. Exp. Tech.* **61** 159
[18] Tolstogouzov A, Aguas H, Ayouchi R, Belykh S F, Fernandes F, Gololobov G P, Moutinho A M C, Schwarz R, Suvorov D V and Teodoro O M N D 2016 *Vacuum* **131** 252
[19] Wilbur P J, Wilson M and Hutchings K J 2007 *Propul. Power* **23** 1049
[20] Escher C, Thomann S, Andreoli C and Fink H W 2006 *Appl. Phys. Lett.* **89** 53513
[21] Owens B B and Argue G R 1967 *Science* **157** 308
[22] Peng H F, Machida N and Shigematsu T 2002 *J. Jpn. Soc. Powder Powder Metall.* **49** 69